Article

Structure

An Atypical MAGUK GK Target Recognition Mode Revealed by the Interaction between DLG and KIF13B

Graphical Abstract

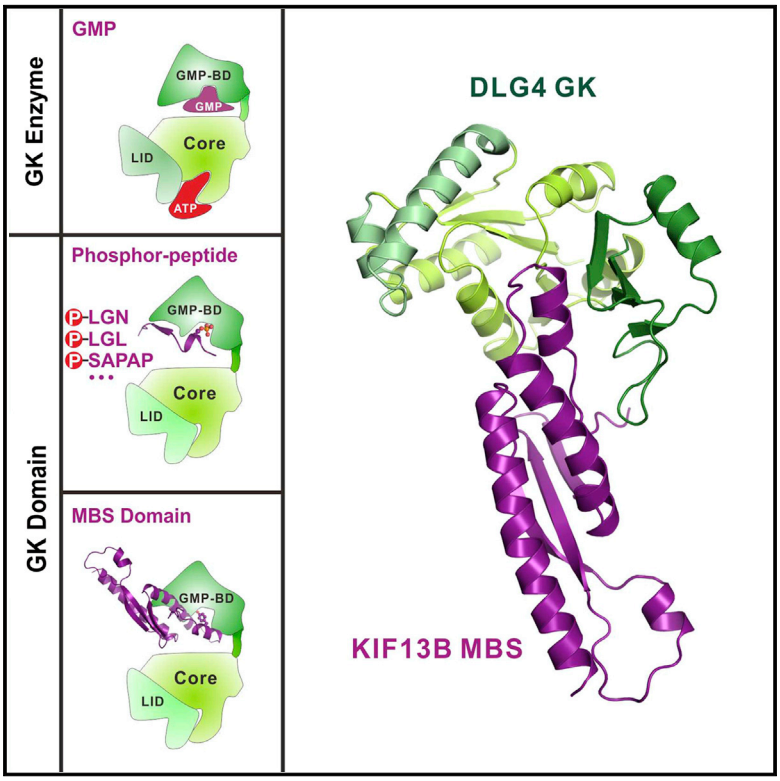

Authors

Jinwei Zhu, Yuan Shang, Yitian Xia, Rongguang Zhang, Mingjie Zhang

Correspondence

jinwei.zhu@sibcb.ac.cn (J.Z.), mzhang@ust.hk (M.Z.)

In Brief

The guanylate kinase (GK) domain of DLG, a membrane-associated guanylate kinase (MAGUK) scaffold protein, binds to the cargo binding tail of the KIF13B kinesin. Zhu et al. find that, unlike other known GK interactions, binding of DLG GK does not require KIF13B phosphorylation, revealing a unique binding mode for MAGUK GK.

Highlights

- KIF13B MBS interacts with DLG GK in a phosphorylation-independent manner
- KIF13B MBS forms a folded domain instead of a linear peptide when bound to DLG GK
- Bindings of KIF13B MBS and phosphor-LGN to DLG GK are mutually exclusive
- Phosphorylation-independent target binding is another general property of MAGUK GK

Accession Numbers

5B64

Zhu et al., 2016, Structure *24*, 1–10
November 1, 2016
http://dx.doi.org/10.1016/j.str.2016.08.008

CellPress

Please cite this article in press as: Zhu et al., An Atypical MAGUK GK Target Recognition Mode Revealed by the Interaction between DLG and KIF13B, Structure (2016), http://dx.doi.org/10.1016/j.str.2016.08.008

Structure
Article

An Atypical MAGUK GK Target Recognition Mode Revealed by the Interaction between DLG and KIF13B

Jinwei Zhu,[1,2,4,*] Yuan Shang,[2,4] Yitian Xia,[1,2] Rongguang Zhang,[1] and Mingjie Zhang[2,3,5,*]
[1]National Center for Protein Science Shanghai, Institute of Biochemistry and Cell Biology, Shanghai Institutes for Biological Sciences, Chinese Academy of Sciences, Shanghai 201210, China
[2]Division of Life Science, State Key Laboratory of Molecular Neuroscience
[3]Center of Systems Biology and Human Health, School of Science and Institute for Advanced Study
Hong Kong University of Science and Technology, Clear Water Bay, Kowloon, Hong Kong, China
[4]Co-first author
[5]Lead Contact
*Correspondence: jinwei.zhu@sibcb.ac.cn (J.Z.), mzhang@ust.hk (M.Z.)
http://dx.doi.org/10.1016/j.str.2016.08.008

SUMMARY

The membrane-associated guanylate kinase (MAGUK) scaffold proteins share a signature guanylate kinase (GK) domain. Despite their diverse functional roles in cell polarity control and synaptic signaling, the currently known mode of action of MAGUK GK is via its binding to phosphorylated short peptides from target proteins. Here, we discover that the GK domain of DLG MAGUK binds to an unphosphorylated and autonomously folded domain within the stalk region (MAGUK binding stalk [MBS] domain) of a kinesin motor KIF13B with high specificity and affinity. The structure of DLG4 GK in complex with KIF13B MBS reveals the molecular mechanism governing this atypical GK/target recognition mode and provides insights into DLG/KIF13B complex-mediated regulation of diverse cellular processes such as asymmetric cell division. We further show that binding to non-phosphorylated targets is another general property of MAGUK GKs, thus expanding the mechanisms of action of the MAGUK family proteins.

INTRODUCTION

Membrane-associated guanylate kinases (MAGUKs) are a family of scaffold proteins concentrated at the sites of cell-cell junctions, playing critical roles in diverse cellular processes, including establishment and maintenance of cell polarity, cell proliferation and differentiation, and synaptic signal transduction (Elias and Nicoll, 2007; Funke et al., 2005; St Johnston and Ahringer, 2010; Zhu et al., 2016). Discs large homologs (DLGs) are founding members of the MAGUK family proteins, with multiple protein-protein interaction domains capable of organizing many different protein complexes with broad cellular functions. For example, the DLG/LGL/SCRIB ternary complex, often acting cooperatively with the Crb/PALS1/PATJ and the PAR3/PAR6/aPKC complexes, is essential for both the development and maintenance of polarities of cells in diverse tissues (Assemat et al., 2008; Chen and Zhang, 2013; Rodriguez-Boulan and Macara, 2014). Defects in DLG/LGL/SCRIB complex formation lead to loss of cell polarity and cancer formation (Bilder et al., 2000; Humbert et al., 2008). In addition to functioning as cell polarity regulators in epithelia, DLG-mediated protein complexes (e.g., the DLG/LGN complex) are essential for controlling cell-fate specification and epithelial architecture by regulating mitotic spindle orientations both in symmetric and asymmetric cell division, and thus are critical for stem cell development and tissue homeostasis in organs/tissues such as brain, muscle, skin, kidney, etc. (Albertson and Doe, 2003; Ben-Yair et al., 2011; Lu and Johnston, 2013; Morin and Bellaiche, 2011; Williams et al., 2014). Mechanistically, formation of these protein complexes is mediated by the guanylate kinase-like (GK) domain of DLG MAGUK, which evolved from the GK that catalyzes phosphotransfer from ATP to GMP (Johnston et al., 2012; Zhu et al., 2011, 2012). Binding of DLG GK to LGN and lethal giant larvae (LGL) strictly requires phosphorylation of short linear peptide sequences in LGN and LGL. Phosphorylated LGN and LGL peptides occupy the evolutionarily conserved binding sites on DLG GK. Structural biology studies indicated that binding to phospho-proteins is likely to be a common feature for most GK domains of MAGUKs including DLGs, calcium/calmodulin-dependent serine protein kinase (CASK), palmitoylated membrane proteins (MPPs), and membrane-associated guanylate kinase inverted (MAGIs) (Zhu et al., 2011, 2012).

Recently, a spindle capture pathway, which involves the Pins/DLG/Khc73 complex, was identified to play critical roles in the telophase rescue process of asymmetric cell division (ACD) in *Drosophila* neuroblasts (Johnston et al., 2009; Lu and Prehoda, 2013; Siegrist and Doe, 2005). In this context, in addition to phosphorylated Pins, DLG GK also binds to Khc73 (KIF13B or GAKIN in mammals), a kinesin-3 family motor protein concentrated at the plus-end tips of astral microtubules. The Pins/DLG/Khc73 complex, which serves as an adaptor bridging apical cell cortex and astral microtubules, was sufficient to promote the mitotic spindle orientation in *Drosophila* S2 cells engineered with an induced polarity assay system (Johnston et al., 2009). Loss of DLG or Khc73 activity led to oriented cell division defects in neuroblasts (Siegrist and Doe, 2005). In mammals, DLG and KIF13B are also known to interact directly with each other (Asaba

et al., 2003; Bolis et al., 2009; Hanada et al., 2000; Kanai et al., 2014). The interaction between DLG1 and KIF13B has been shown to be required for transporting DLG1 to paranodes of Schwann cells and for proper myelination of axons (Bolis et al., 2009). In neurons, KIF13B is enriched at the tips of growing axons and can promote axon formation (Yoshimura et al., 2010). Mutations of KIF13B have been implicated in autism (Li et al., 2015). The formation of the DLG1/KIF13B complex has also been indicated for polarized transport of DLG1 in epithelial cells and T lymphocytes (Asaba et al., 2003; Hanada et al., 2000). Moreover, DLG1 has been shown to function as the adaptor involved in KIF13B-mediated endocytosis of low-density lipoprotein receptor-related protein 1 (LRP1) (Kanai et al., 2014). However, little is known about the molecular basis governing DLG/KIF13B complex formation and the potential connections of this interaction with the reported phosphorylation-dependent binding of DLG GK to targets such as LGN, SAP90/PSD-95-associated proteins (SAPAPs), and LGL (Zhu et al., 2011, 2014).

In this work, we confirmed that the interaction between DLG GK and KIF13B does not require phosphorylation of KIF13B. Instead of binding to a short phosphorylated linear peptide, DLG GK binds to an autonomously folded domain of KIF13B with high affinity. The structure of DLG GK in complex with its binding domain from KIF13B not only reveals the mechanism governing this non-phosphorylated target binding mode of DLG GK but also explains the exquisite specificity of DLG in recognizing KIF13B instead of the highly homologous KIF13A. Finally, we provide evidence that binding to non-phosphorylated but folded domains is another general target recognition mechanism of the GK domains from the MAGUK family of scaffold proteins.

RESULTS

Binding of KIF13B MBS to DLG GK Does Not Require Phosphorylation of KIF13B MBS

An earlier study has shown that DLG binds to Khc73 in *Drosophila* (Siegrist and Doe, 2005). In mammals, DLG can specifically interact with KIF13B, and the interaction was mapped to the GK domain of DLG and the central coiled-coil region of KIF13B (aa 607–831) (Asaba et al., 2003; Hanada et al., 2000) (Figure 1A). Detailed sequence analysis showed that KIF13B lacks the consensus GK-binding sequence derived from the known phosphorylated targets of MAGUKs such as LGN, SAPAP, and LGL (Zhu et al., 2011, 2014), suggesting that the binding of DLG GK to KIF13B may adopt a mode distinct from that of phospho-target binding. We first confirmed the DLG/KIF13B interaction by showing that GST-DLG4 GK binds robustly to a KIF13B stalk region fragment (aa 586–847) (Figure 1B). Using a truncation-based approach, a 122-residue fragment of KIF13B (aa 677–798; referred as to the MAGUK binding stalk domain [MBS] domain) was shown to be the minimal GK-binding domain (Figures 1B and 1C). Further truncations either at the N or C terminus of MBS abolished its binding to DLG4 GK (Figure 1B). We further demonstrated that DLG4 GK and KIF13B MBS form a stable 1:1 stoichiometric complex (Figure 1D). Quantitative binding assays showed that KIF13B MBS binds to DLG4 GK with a dissociation constant (K_d) of ~70 nM, an affinity a few fold stronger than that of phospho-target binding (e.g., K_d ~330 nM in binding to pLGN and ~240 nM to pSAPAP) (Zhu et al., 2011) (Figure 1E). In sharp contrast to previously reported phosphorylation-dependent target binding, unphosphorylated KIF13B MBS interacts directly with DLG GK.

Overall Structure of the DLG4 GK/KIF13B MBS Complex

To elucidate the molecular details governing the DLG/KIF13B interaction, we solved the crystal structure of the DLG4 GK/KIF13B MBS complex at 2.7-Å resolution (Table 1). Consistent with our biochemical data shown in Figure 1C, each asymmetric unit of the crystal contains one complex with 1:1 stoichiometry (Figures 2A and 2B). The overall structure of the DLG4 GK/KIF13B MBS complex has a mushroom-like shape, with DLG4 GK and KIF13B MBS constituting the cap and stalk of the mushroom, respectively (Figure 2A). In the complex, DLG4 GK adopts the typical GK domain architecture, comprised of the CORE, LID, and GMP-binding (GMP-BD) subdomains (Figure 2B). Unexpectedly, KIF13B MBS forms a mixed α helix/β strand fold instead of a previously predicted coiled-coil conformation, and binds to the previously identified phospho-peptide binding site of DLG GK (Figure 2, see below for details). As such, although with totally different structures, the KIF13B binding pocket and the phospho-target binding pocket on DLG GK partially overlap (Figures 2B and 2C).

Structure of the KIF13B MBS Domain

All members of the kinesin-3 family motors (KIF1, KIF13, and KIF14) contain an MBS domain following the Forkhead-associated (FHA) domain. In the complex with DLG GK, KIF13B MBS adopts a compact folded structure, composed of four α helices (αA–D) and three antiparallel β strands (βA–C) (Figures 3A and 3B). Amino acid sequence alignment analysis of the MBS domains from different members of the kinesin-3 motors shows that both the secondary structures (except for αD) and the key residues forming the folding core of KIF13B MBS are highly conserved (Figures 3A and S1), indicating that all other kinesin-3 family members likely contain a similar folded MBS domain observed in KIF13B.

Analysis of the surface properties of KIF13B MBS reveals a prominent negatively charged surface situated between αC and αD (Figures 3C and S1). This negative charged surface is directly involved in the binding of KIF13B MBS to DLG GK. On the opposite side of this negatively charged surface, KIF13B MBS contains a large solvent-exposed hydrophobic surface surrounded by several positively charged residues (Figure 3C). It is noted that the majority of these hydrophobic residues are conserved among the kinesin-3 family proteins (Figure S1), suggesting that this hydrophobic surface of MBS may be a common cargo binding site for all the kinesin-3 motors.

The DLG4 GK/KIF13B MBS Interface

The robust interaction between DLG4 GK and KIF13B MBS is mainly mediated by extensive polar and hydrophobic interactions, burying a total of 825 $Å^2$ of accessible surface area (Figures 4A and 4B). A large number of polar residues from the C-terminal half of αC and throughout the entire αD of KIF13B MBS contribute to the binding to DLG4 GK (Figures 4B and S2). Specifically, the side chain of $Y783_{MBS}$ from αD forms a

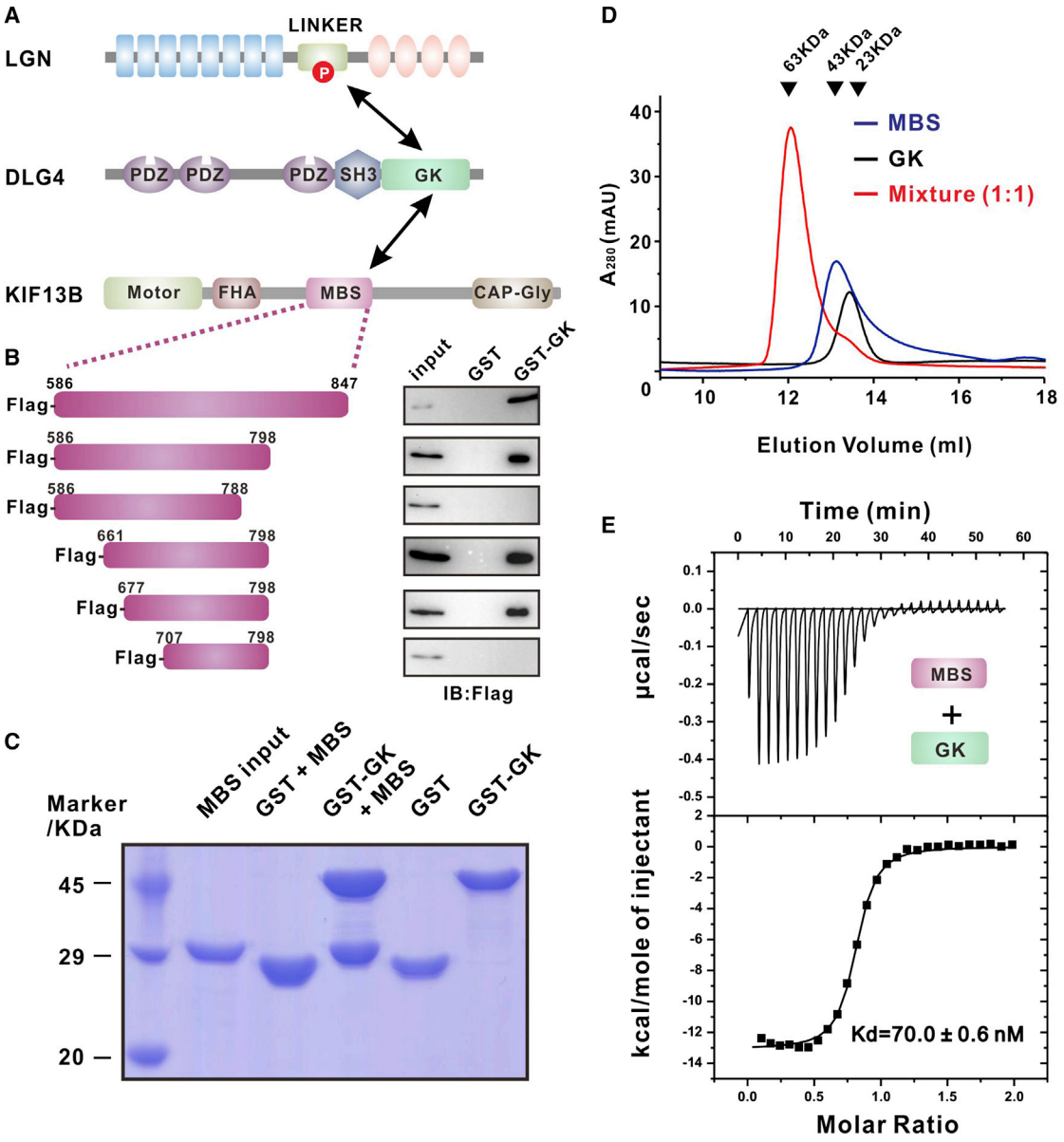

Figure 1. KIF13B MBS Directly Interacts with DLG GK

(A) A schematic diagram showing the domain organization of LGN, DLG4, and KIF13B. Interactions between LGN, DLG4, and KIF13B are indicated by a two-way arrow.

(B) GST-pull-down-assay-based analyses of the interactions between various Flag-tagged KIF13B fragments and DLG4 GK expressed in heterologous cells.

(C) Pull-down assay showing that GST-DLG4 GK robustly binds to Trx-KIF13B MBS.

(D) Analytical gel filtration analysis showing that KIF13B MBS and DLG4 GK formed a 1:1 stoichiometric complex. The elution volumes of the molecular mass standards are indicated at the top of the panel.

(E) Isothermal titration calorimetry of purified Trx-KIF13B MBS and Trx-DLG4 GK, indicating a complex with a dissociation constant of 70.0 ± 0.6 nM.

hydrogen-bonding interaction network with $R571_{GK}$, $Y573_{GK}$, and $E769_{MBS}$ from αC. The side chain of $E769_{MBS}$ also forms hydrogen bonds with $Y604_{GK}$ and $N605_{GK}$ (Figures 4B and S3). The side chain of $S561_{GK}$ forms hydrogen bonds with $K785_{MBS}$ and $R786_{MBS}$, the latter in turn participates in the hydrogen bond network with the main chains of $R578_{GK}$ and $D579_{GK}$. Several charge-charge interactions also contribute to the DLG4/KIF13B interaction (Figures 4B and S3). For example, $R781_{MBS}$ forms a salt bridge with $D629_{GK}$, and $R759_{MBS}$ forms a salt bridge with $E572_{GK}$. Consistent with these structural analyses, mutations that disrupt these polar interactions invariably weakened or even disrupted the DLG4/KIF13B interaction (Figure 4C). Notably, the R786E mutant that disrupted the interaction between the MBS domain and the GK domain also abolished the association between DLG4 GK and the full-length KIF13B, suggesting that the MBS domain is the necessary and sufficient region for KIF13B to bind to DLG4 GK (Figure 4D). In addition to these polar interactions, the hydrophobic residues from αD

Table 1. Data Collection and Refinement Statistics

	DLG4 GK/KIF13B MBS
Data Collection	
Space group	I4
Cell dimensions	
a, *b*, *c* (Å)	116.279, 116.279, 72.029
Resolution (Å)	50.00–2.70 (2.75–2.70)
R_{merge} [a]	6.9 (68.2)
$I/\sigma I$	25.8 (2.8)
Completeness (%)	97.8 (99.2)
Redundancy	3.8 (4.0)
Refinement	
Resolution (Å)	36.77–2.70 (2.80–2.70)
No. of reflections in refinement	13,024 (1,322)
No. of reflections in R_{free}	643 (63)
R_{work} [b]/R_{free} [c]	18.65 (29.73)/24.31 (36.99)
No. atoms	
Protein	2,277
Ligand/ion	42
Water	29
B factors	
Protein	83.9
Ligand/ion	124
Water	72.3
RMSD	
Bond length (Å)	0.008
Bond angle (°)	1.09
Ramachandran plot (%)	
Favored region	97.60
Allowed region	2.40
Outlier region	0

Values in parentheses are for highest-resolution shell.

[a] $R_{merge} = \sum|I_i - I_m|/\sum I_i$, where I_i is the intensity of the measured reflection and I_m is the mean intensity of all symmetry-related reflections.

[b] $R_{work} = \Sigma||F_{obs}| - |F_{calc}||/\Sigma|F_{obs}|$, where F_{obs} and F_{calc} are observed and calculated structure factors in the refinement.

[c] $R_{free} = \Sigma_T||F_{obs}| - |F_{calc}||/\Sigma_T|F_{obs}|$, where T is a test dataset of about 5% of the total reflections randomly chosen and set aside prior to refinement.

of KIF13B MBS, such as $C773_{MBS}$, $V779_{MBS}$, $S780_{MBS}$, and $Y783_{MBS}$, insert into the hydrophobic pocket of DLG4 GK formed by $P564_{GK}$, $Y580_{GK}$, $Y604_{GK}$, $Y609_{GK}$, and $T611_{GK}$, further enhancing their binding (Figures 4B and S3). Parallel to the above analysis, substitution of $Y783_{MBS}$ with Ala decreased binding of KIF13B MBS to DLG4 GK by ~200 fold. Substitution of $Y604_{GK}$ with Ala abolished the interaction (Figure 4C).

Since most of the binding sites on KIF13B MBS are located at αD and binding of GK to phospho-targets requires only a short peptide fragment, one might wonder whether the αD of MBS may provide the majority of the binding energy for the DLG4/KIF13B interaction (Figure 4B). To test this possibility, we purified the KIF13B fragment encompassing the αD of MBS (KIF13B-αD, aa 774–793; Figure S4A) and measured its interaction with DLG4 GK. KIF13B-αD did not bind to DLG4 GK (Figure S4B), suggesting that the integration of αD to the folded MBS domain structure is essential for KIF13B to bind to DLG4 GK. Consistent with this interpretation, substitution of $F784_{MBS}$ (a key residue for coupling αD to the folding core of MBS but not directly involved in DLG4 GK binding; Figure S4C) into Gly abolished the DLG4 GK/KIF13B MBS interaction (Figure S4D). We chose to substitute $F784_{MBS}$ with a Gly as the residue at the corresponding position of KIF13A MBS is a Gly (Figure S4A). Interestingly, key residues on αD of MBS involved in the DLG4/KIF13B interaction are not conserved among the kinesin-3 family proteins (Figure S4A), indicating that binding to DLG GK is likely to be highly specific for KIF13B. Indeed, no detectable binding could be observed between KIF13A MBS and DLG4 GK (Figure 4E), although the rest of their MBS regions are highly similar. The above observation also indicates that small amino acid sequence variation in the MBS regions can diversify the cargo binding capacities of the kinesin-3 motors.

Binding of KIF13B MBS and Phospho-LGN to DLG GK Is Mutually Exclusive

We next asked whether DLG GK can bind to pLGN and KIF13B simultaneously. Firstly, we compared the structures of DLG1/pLGN and DLG4/KIF13B complexes. The conformation of GK in the DLG1/pLGN and DLG4/KIF13B complexes is highly similar (root-mean-square deviation [RMSD] = 0.79 Å). The N-terminal half of the pLGN peptide (which also forms an α helix) and the αD of KIF13B MBS occupy the same region in the DLG GK target binding pocket (Figure 5A). A close-up view of the GK domain in two complexes reveals that several residues from the GMP-BD subdomain of GK are critical for both binding to pLGN and MBS (Figures 5B and 5C). In particular, $Y783_{MBS}$ occupies the same position as the phosphoserine (S0) in pLGN, and $R786_{MBS}$ and $R(-2)_{pLGN}$ show the same binding mode in both complex structures (Figure 5B). The above analysis indicates that DLG GK cannot bind to pLGN and KIF13B MBS simultaneously. Indeed, pLGN can compete with KIF13B MBS in binding to DLG GK in a dose-dependent manner (Figure 5D). Thus, the bindings of KIF13B MBS and phospho-LGN to DLG GK are mutually exclusive.

DISCUSSION

The most important finding of this study is that the high-affinity binding of KIF13B MBS to DLG GK does not require phosphorylation of KIF13B. Our study suggests that, in addition to recognizing phosphorylated targets, MAGUK GKs can also recognize non-phosphorylated targets. Since the interaction between DLG GK and KIF13B MBS does not need the KIF13B to be phosphorylated, this interaction would be constitutively present as long as the two proteins can meet each other. In contrast, bindings of MAGUK GKs to targets such as LGN, SAPAP, and LGL require these MAGUK targets to be phosphorylated, and thus their interactions are regulated events. It should be pointed out that the binding of DLG GK to unphosphorylated KIF13B does not necessarily mean that the interaction cannot be regulated by phosphorylation. For example, Tyr783 in KIF13B MBS plays a critical role in the formation of the GK/MBS complex (Figures 4B and 4C). Substitution of Tyr783 with Glu completely disrupted the interaction between KIF13B MBS and DLG GK (Figure S5),

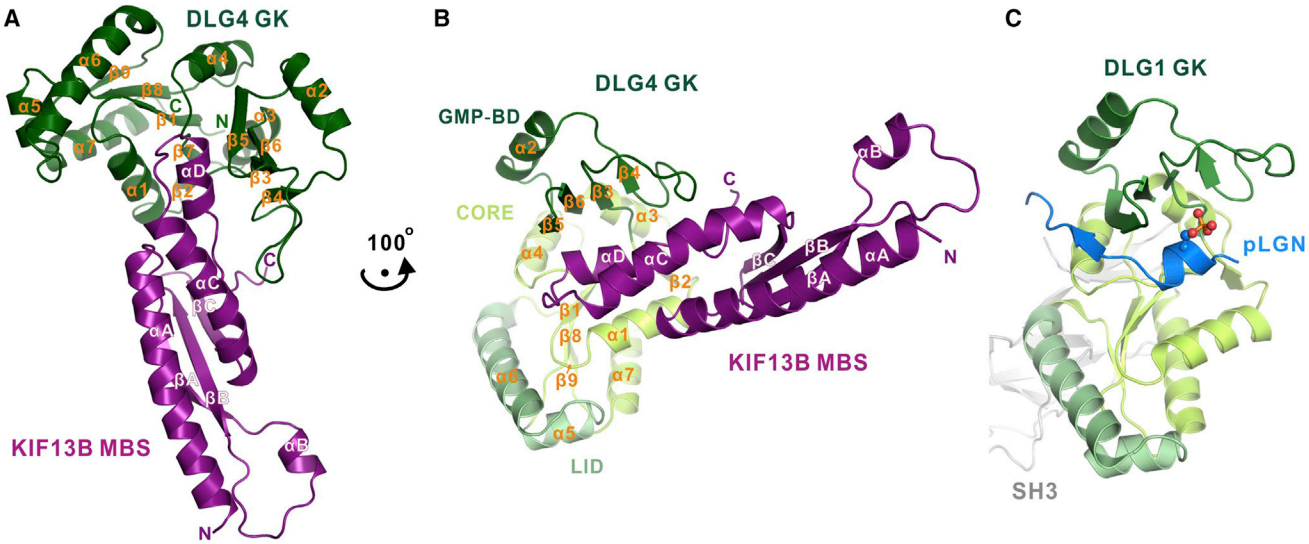

Figure 2. Overall Structure of the DLG4 GK/KIF13B MBS Complex

(A) Ribbon diagram representation of the DLG4 GK/KIF13B MBS complex structure. DLG4 GK and KIF13B MBS are colored in green and purple, respectively.

(B) The MBS domain of KIF13B interacts with the concave pocket formed by the GMP-binding domain (GMP-BD) and the CORE subdomains of DLG4 GK. The GMP-BD, CORE, and LID subdomains of DLG4 GK are shown in green, light green, and pale green, respectively.

(C) Ribbon diagram representation of the DLG1 SH3-GK/phospho-LGN (pLGN) complex structure (PDB: 3AUT). The GMP-BD, CORE, and LID subdomains of DLG1 GK are shown in the same colors as in (B). The pLGN peptide is shown in blue with the phosphate group shown in red using the stick-and-ball model. The SH3 domain is shown in gray.

suggesting that phosphorylation of Tyr783 of KIF13B can disrupt its interaction with DLG.

The residues responsible for KIF13B MBS binding are essentially completely conserved among the members of the DLG family MAGUKs (Figure 5C). Therefore, all DLGs are expected to bind to KIF13B MBS, and indeed DLG1 GK was also found to bind to KIF13B MBS with high affinity (data not shown). We noted that DLG3 has a Phe at the position corresponding to Tyr604 of DLG4. The hydroxyl group of Tyr604 of DLG4 GK forms a hydrogen-bonding network with $E769_{MBS}$ and $N605_{GK}$, in addition to hydrophobic interactions (Figure 4B). Interestingly, although it does still bind, DLG3 GK binds to KIF13B MBS with an affinity ~400-folder weaker than that of DLG4 GK (data not shown), highlighting the importance of the key residues in the interaction interface for DLG4/KIF13B complex formation. We also notice that MPP5 (PALS1), another MAGUK member, shares essentially the same KIF13B MBS binding residues as DLGs. Satisfyingly, MPP5 (PALS1) GK was found to bind to KIF13B MBS with a strength comparable with that of DLG GK (Figure 5E). The residues corresponding to those in DLG GK for KIF13B MBS binding in CASK and MAGIs contain a small degree of variation. Interestingly, neither CASK GK nor MAGI3 GK showed detectable binding to KIF13B MBS (Figure 5E), indicating that binding of non-phosphorylated targets by MAGUK GKs may have higher specificity with respect to the mode observed in phosphorylation-dependent target binding. In conclusion, the findings described in this study significantly expand the target recognition mechanisms of the MAGUK GK domains. Given the extremely broad functional roles of MAGUKs in all multi-cellular eukaryotes, our results are likely to be helpful for future functional studies on this family of scaffold proteins in general.

Controlled coordination between the mitotic spindle orientation and intrinsic cell polarity cue(s) is critical for ACD during tissue development (Gonczy, 2008; Knoblich, 2008, 2010; Morrison and Kimble, 2006; Siller and Doe, 2009; Williams and Fuchs, 2013). The NuMA/LGN/DLG/Gα pathway has been shown to be critical to link the mitotic spindle complex to the cell polarity complex at membrane cortices in many tissue types (Kulukian and Fuchs, 2013; Lu and Johnston, 2013; Siller and Doe, 2009; Zhu et al., 2012). Another pathway that involves the LGN/DLG/KIF13B complex (the Pins/DLG/Khc73 in *Drosophila*) has also been shown to be essential for coordinating cell polarity and mitotic spindle orientation (Johnston et al., 2009; Siegrist and Doe, 2005). DLG is involved in both pathways; one is via binding to phosphorylated LGN (Pins) and the other is via constitutive binding to KIF13B (Khc73). Although the two DLG targets bind to DLG GK with totally different molecular mechanisms, their binding sites on DLG GK largely overlap. Therefore, phospho-LGN and KIF13B bind to DLG GK in a mutually exclusive manner (Figure 5D). How might the above two pathways function together in orchestrating spindle orientation during ACD? One likely mechanism is via formation of DLG oligomers at the cell cortices, so that DLG molecules can simultaneously engage phospho-LGN and KIF13B (Figure 6). DLGs and other MAGUK members are known to be able to form oligomers (Tavares et al., 2001; Zhu et al., 2016). Mechanistically, the SH3 domain and GK domain of MAGUKs can form domain-swapped intermolecular dimers or high-order oligomers (Hara et al., 2015; Li et al., 2014; McGee et al., 2001; Tavares et al., 2001; Zhu et al., 2016). Alternatively, DLG may adopt a sequential target binding model. In this model, the Insc/Par/LGN/Gα pathway initiates DLG cortical polarization via the DLG/pLGN interaction at prometaphase/metaphase. During metaphase, astral microtubule

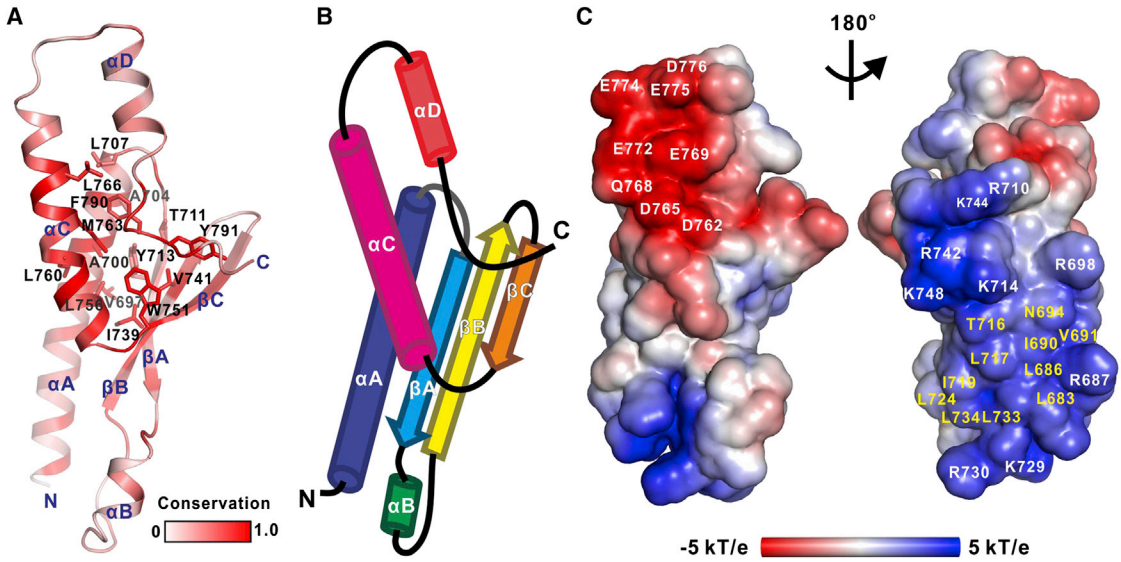

Figure 3. Structure of the KIF13B MBS Domain

(A) View of the KIF13B MBS domain showing the hydrophobic core of the structure. The conservation score was obtained based on the sequence alignment in Figure S1 using the Scorecons server (Valdar, 2002).

(B) Topology diagram showing the fold of the KIF13B MBS domain.

(C) Surface analysis of KIF13B MBS reveals a highly negatively charged surface and a hydrophobic pocket surrounded by a positive charged surface on the back side. The figure was drawn using the electrostatic surface charge potential map. See also Figure S1.

plus-end-enriched KIF13B takes over to bind to DLG to facilitate cortical astral microtubule capture. This process may be accompanied by de-phosphorylation of LGN. Thus, DLG/KIF13B interaction may provide a physical connection between the astral microtubule and Gα/LGN/NuMA/dynein complex to orchestrate fully activated spindle orientation in ACD (Lu and Johnston, 2013; Lu and Prehoda, 2013; Siller and Doe, 2009) (Figure 6). It should be emphasized that the structural data in the current study, together with data already published, prompted us to suggest possible models on how DLG may function in interfacing the cortical polarity complex with the mitotic spindle orientation complex during ACD. Further studies are required to test the models hypothesized in Figure 6.

EXPERIMENTAL PROCEDURES

Protein Preparation

The MBS domain (aa 677–798) of mouse KIF13B was PCR-amplified from the mouse brain cDNA library and cloned into modified pET32a vectors. The rat DLG4 GK domain (aa 531–713) and various mutants (Figure 4C) were individually cloned into modified pET15b or pET32a vectors. All the mutations were created using the standard PCR-based method and confirmed by DNA sequencing. Recombinant proteins were expressed in *Escherichia coli* BL21 (DE3) host cells at 16°C and were purified by using Ni^{2+}-NTA agarose affinity chromatography followed by size-exclusion chromatography. For GST pull-down experiments, GK domains of MAGUK family proteins (i.e., DLG4, MPP5, CASK, and MAGI3) were fused to the C terminus of GST using the pGEX-4T-1 vector and purified by GSH-Sepharose affinity chromatography.

Size-Exclusion Chromatography

Size-exclusion chromatography experiments were carried out on an AKTA FPLC system (GE Healthcare). Proteins at concentrations of 10–20 μM in a volume of 100 μL were loaded on a Superose 12 10/300 GL column 20 (GE Healthcare) equilibrated with buffer containing 50 mM Tris (pH 8.0), 100 mM NaCl, 1 mM DTT, and 1 mM EDTA. Protein elution was detected by absorbance at 280 nm.

GST Pull-Down Assay

GST-tagged DLG4 GK (2 nM) was incubated with fresh purified Trx-KIF13B MBS at a molar ratio of 1:5 for 1 hr at 4°C. The mixture was then loaded onto 30 μL GSH-Sepharose 4B slurry beads in assay buffer (50 mM Tris [pH 8.0], 100 mM NaCl, 1 mM DTT, and 1 mM EDTA) for 0.5 hr at 4°C. After washing three times, the proteins captured were eluted by boiling, resolved by 15% SDS-PAGE, and detected by Coomassie brilliant blue staining.

GST-tagged DLG4 (or MPP5, CASK, MAGI3) GKs (2 nM) were first loaded onto 30 μL GSH-Sepharose 4B slurry beads in assay buffer (50 mM Tris [pH 8.0], 100 mM NaCl, 1 mM DTT, and 1 mM EDTA). The GST fusion protein-loaded beads were then incubated with Myc-tagged human KIF13B (full length or mutant) and various Flag-tagged KIF13B MBS or KIF13A MBS fragments for 2 hr at 4°C. After washing three times, the proteins captured were eluted by boiling, resolved by 15% SDS-PAGE, and detected by western blot using anti-Myc (DSHB) or anti-Flag antibody (Sigma).

Isothermal Titration Calorimetry

Isothermal titration calorimetry measurements were performed on a VP-ITC calorimeter (MicroCal) at 25°C. All protein samples were in 50 mM Tris (pH 8.0), 100 mM NaCl, 1 mM EDTA, and 1 mM DTT buffer. The titration process was performed by injecting 10 μL aliquots of the MBS fragments into GK proteins at time intervals of 2 min to ensure that the titration peak returned to the baseline. The titration data were analyzed using the Origin7.0 program from MicroCal.

Crystallography

Crystals of the DLG4 GK/KIF13B MBS complex (10 mg/mL) were obtained by the hanging-drop vapor-diffusion method at 18°C. The GK/MBS complex crystals were grown in 1.0 M ammonium sulfate, 0.1 M HEPES (pH 7.0), 0.5% w/v polyethylene glycol 8000. Crystals were soaked in crystallization solution containing 25% glycerol for cryo-protection. The diffraction data were collected at 0.97915 Å from a single crystal from Shanghai Synchrotron Radiation Facility. The data were integrated and scaled using HKL2000 (Otwinowski and Minor, 1997). Molecular replacement was used to solve the complex structure using

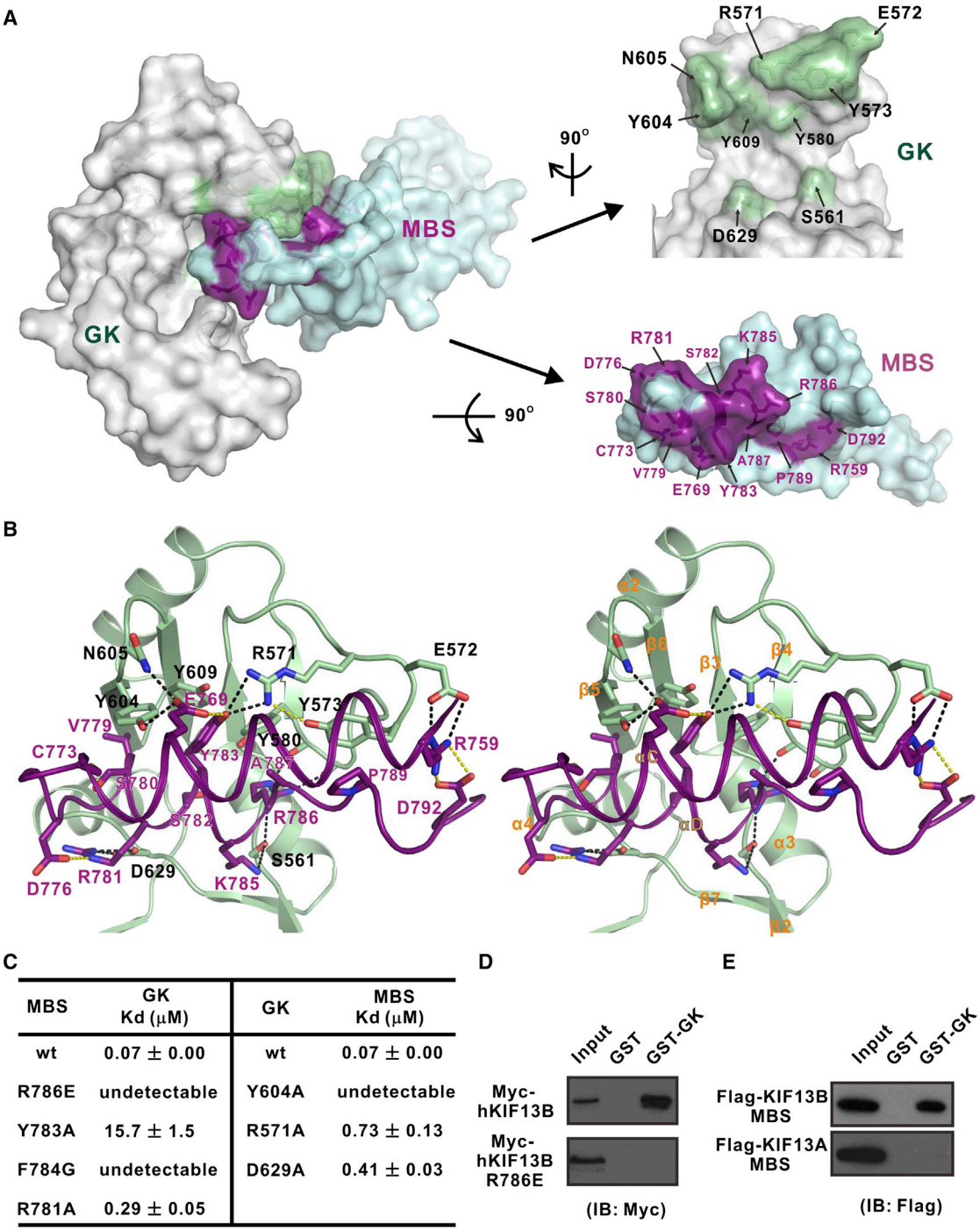

MBS	GK Kd (μM)	GK	MBS Kd (μM)
wt	0.07 ± 0.00	wt	0.07 ± 0.00
R786E	undetectable	Y604A	undetectable
Y783A	15.7 ± 1.5	R571A	0.73 ± 0.13
F784G	undetectable	D629A	0.41 ± 0.03
R781A	0.29 ± 0.05		

Figure 4. The Interface of the DLG4 GK/KIF13B MBS Complex

(A) Semitransparent surface representation of the GK/MBS complex with the underlying backbone structure showing (left). The flipped open interaction interface of the GK/MBS complex is also shown (right). GK and MBS have been rotated and separated as indicated by the arrows. Residues involved in binding to MBS on GK are shown in pale green. Residues involved in binding to GK on MBS are shown in purple.

(B) Detailed interface of the GK/MBS complex in stereo view. Dotted lines denote hydrogen bonds and salt bridge interactions.

(C) Summary of the binding between the wild-type and various DLG4 GK and KIF13B MBS mutants derived from isothermal titration calorimetry analyses.

(D) GST pull-down assay showed that DLG4 GK binds to full-length KIF13B but not the R786E mutant.

(E) GST pull-down assay showed that DLG4 GK specifically binds to KIF13B MBS but not KIF13A MBS. See also Figures S2–S4.

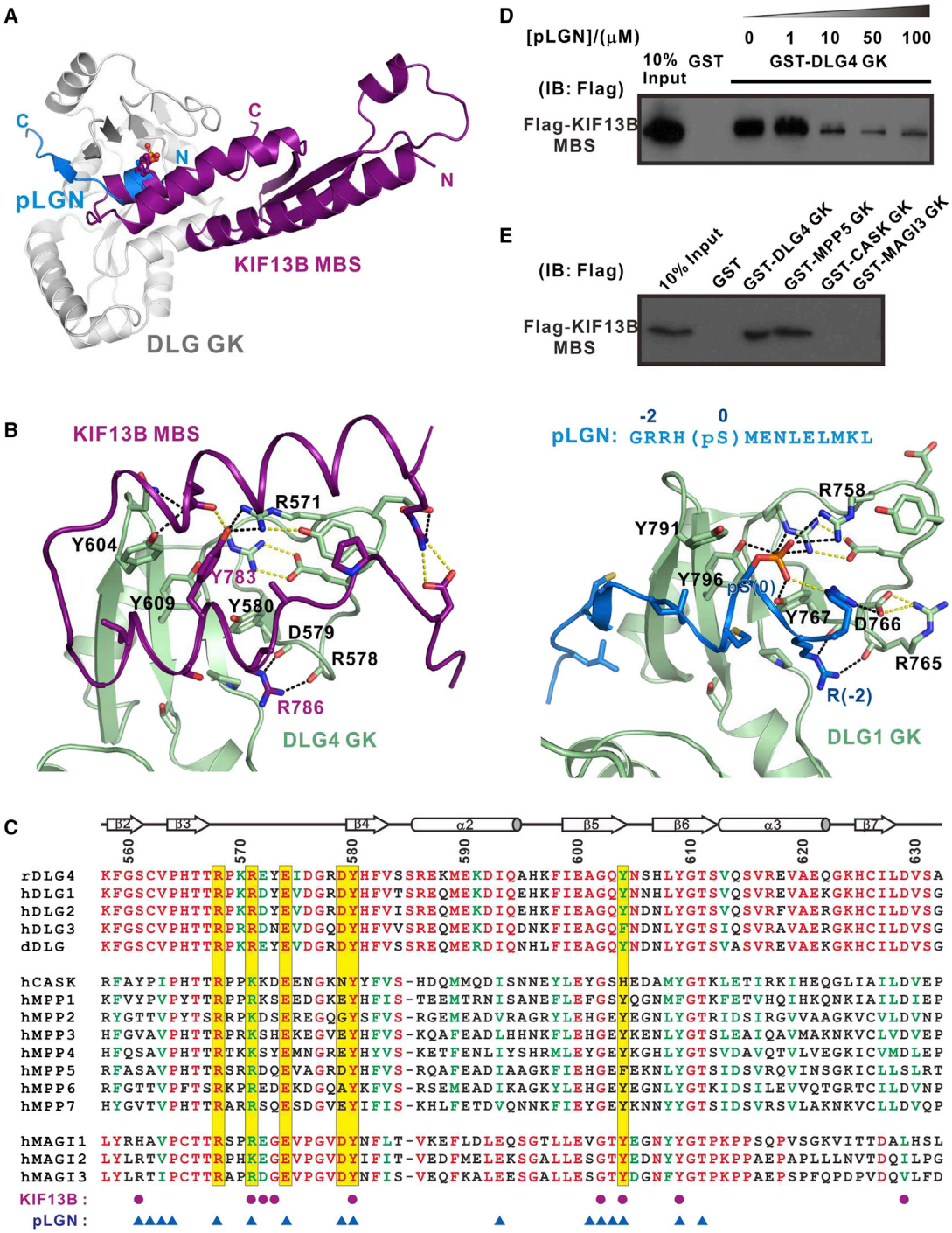

Figure 5. Competitive Binding of KIF13B and pLGN to DLG GK

(A) Ribbon diagram representation showing the superposition of the GK_{DLG1}/pLGN (PDB: 3UAT) and GK_{DLG4}/MBS complexes. The pLGN peptide is shown in blue with the phosphate group shown in red using the stick-and-ball model. The MBS domain of KIF13B is shown in purple. The side chain of $Y783_{MBS}$ is also shown in the stick-and-ball model.

(B) Comparison of the GK_{DLG1}/pLGN and GK_{DLG4}/MBS interfaces. A selected set of residues of GK, which are involved in binding both pLGN and MBS, are drawn in the stick model. pLGN and MBS are shown in blue and purple, respectively.

(C) Structure-based sequence alignment of the GMP-BD subdomains of GKs of MAGUK family proteins. Key residues involved in binding to KIF13B MBS and pLGN are indicated with purple dots and blue triangles, respectively. Residues coordinating the phosphate group of pLGN are highlighted in yellow. Highly conserved and conserved residues are colored in red and green, respectively.

(D) In vitro competition binding assay shows that pLGN dose-dependently inhibits the interaction between KIF13B MBS and DLG4 GK.

(E) GK domains of DLG4 and MPP5 (PALS1) but not CASK and MAGI3 bind to KIF13B MBS.

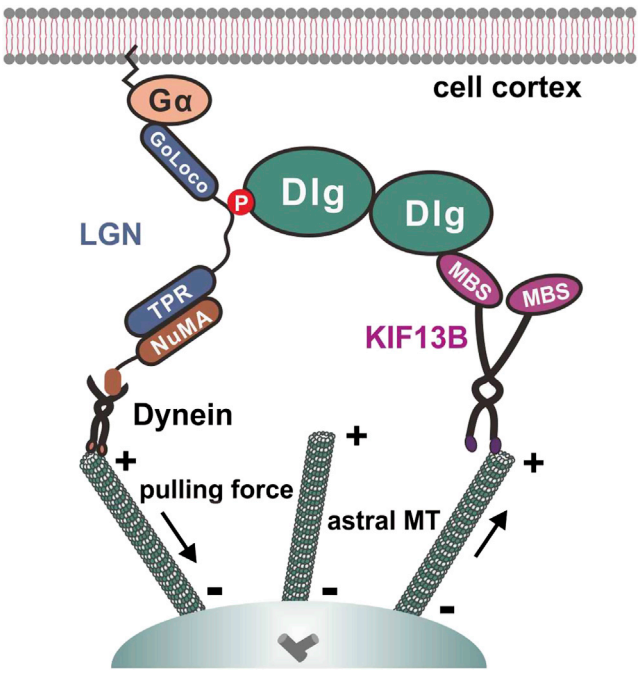

Figure 6. Proposed Model for the DLG/KIF13B Complex in the Spindle Orientation of ACD

During prometaphase/metaphase, cell intrinsic polarity cue(s) initiates cortical enrichment of the Insc/PAR/LGN/Gα complex, which in turn induces polarization of DLG at the apical cortex (via phosphorylation-dependent binding of LGN to DLG GK). Later, astral microtubule (astral MT) plus-end localized KIF13B facilitates the cortical microtubule capture pathway via direct interaction with DLG GK. Given the competitive binding of phospho-LGN and KIF13B to DLG described in this study, DLG cannot simultaneously bind to LGN and KIF13B. DLGs may form high-order oligomers via the intermolecular interactions between the SH3 domain and GK domain, thus linking the phospho-LGN and KIF13B. Alternatively, DLG may adopt a sequential target binding model. Insc/PAR/LGN/Gα first recruits DLG to the apical cortex. Later, KIF13B takes over to interact with DLG, which provides an anchor site for astral MT at the cell cortex.

the structure of DLG4 GK (PDB: 1JKW) as the search model with the software suites in Phaser (McCoy et al., 2007) in CCP4 (Winn et al., 2011). The structure of the MBS domain was manually built guided by the $2F_o - F_c$ map (contoured at 1σ) iteratively. Refinements were carried out using phenix.refinement (Adams et al., 2010). Coot (Emsley et al., 2010) was used for model building and modifications. The structural figures were prepared by PyMOL (www.pymol.org).

Statistical Methods

This study does not involve statistical methods.

ACCESSION NUMBERS

The atomic coordinates of the DLG4 GK/KIF13B MBS complex have been deposited in the PDB under the accession code PDB: 5B64.

SUPPLEMENTAL INFORMATION

Supplemental Information includes five figures and can be found with this article online at http://dx.doi.org/10.1016/j.str.2016.08.008.

AUTHOR CONTRIBUTIONS

Conceptualization, J.Z. and M.Z.; Methodology, J.Z. and Y.S.; Investigation, J.Z., Y.S., and Y.X.; Writing, J.Z., Y.S., and M.Z.; Review & Editing, J.Z., Y.S., R.Z., and M.Z.; Funding Acquisition, J. Z. and M.Z.; Supervision, R.Z. and M.Z.; Coordination, M.Z.

ACKNOWLEDGMENTS

We thank the Shanghai Synchrotron Radiation Facility (SSRF) BL18U1 and BL17U1 for X-ray beam time. We also thank Dr. Hiroaki Miki at Osaka University for providing us with the full-length Myc-tagged KIF13B gene. This work was supported by grants from RGC of Hong Kong (664113, 16103614, AoE-M09-12, and T13-607/12R), a grant from the Asian Foundation for Cancer Research (AFCR14SC01), and a 973 program grant from the Minister of Science and Technology of China (2014CB910204) to M.Z.; and a grant (31470733) from the National Natural Science Foundation of China to J.Z. M.Z. is a Kerry Holdings Professor in Science and a Senior Fellow of IAS at HKUST.

Received: May 22, 2016
Revised: July 14, 2016
Accepted: August 4, 2016
Published: September 15, 2016

REFERENCES

Adams, P.D., Afonine, P.V., Bunkoczi, G., Chen, V.B., Davis, I.W., Echols, N., Headd, J.J., Hung, L.W., Kapral, G.J., Grosse-Kunstleve, R.W., et al. (2010). PHENIX: a comprehensive Python-based system for macromolecular structure solution. Acta Crystallogr. D Biol. Crystallogr. *66*, 213–221.

Albertson, R., and Doe, C.Q. (2003). Dlg, Scrib and Lgl regulate neuroblast cell size and mitotic spindle asymmetry. Nat. Cell Biol. *5*, 166–170.

Asaba, N., Hanada, T., Takeuchi, A., and Chishti, A.H. (2003). Direct interaction with a kinesin-related motor mediates transport of mammalian discs large tumor suppressor homologue in epithelial cells. J. Biol. Chem. *278*, 8395–8400.

Assemat, E., Bazellieres, E., Pallesi-Pocachard, E., Le Bivic, A., and Massey-Harroche, D. (2008). Polarity complex proteins. Biochim. Biophys. Acta *1778*, 614–630.

Ben-Yair, R., Kahane, N., and Kalcheim, C. (2011). LGN-dependent orientation of cell divisions in the dermomyotome controls lineage segregation into muscle and dermis. Development *138*, 4155–4166.

Bilder, D., Li, M., and Perrimon, N. (2000). Cooperative regulation of cell polarity and growth by *Drosophila* tumor suppressors. Science *289*, 113–116.

Bolis, A., Coviello, S., Visigalli, I., Taveggia, C., Bachi, A., Chishti, A.H., Hanada, T., Quattrini, A., Previtali, S.C., Biffi, A., et al. (2009). Dlg1, Sec8, and Mtmr2 regulate membrane homeostasis in Schwann cell myelination. J. Neurosci. *29*, 8858–8870.

Chen, J., and Zhang, M. (2013). The Par3/Par6/aPKC complex and epithelial cell polarity. Exp. Cell Res. *319*, 1357–1364.

Elias, G.M., and Nicoll, R.A. (2007). Synaptic trafficking of glutamate receptors by MAGUK scaffolding proteins. Trends Cell Biol. *17*, 343–352.

Emsley, P., Lohkamp, B., Scott, W.G., and Cowtan, K. (2010). Features and development of Coot. Acta Crystallogr. D Biol. Crystallogr. *66*, 486–501.

Funke, L., Dakoji, S., and Bredt, D.S. (2005). Membrane-associated guanylate kinases regulate adhesion and plasticity at cell junctions. Annu. Rev. Biochem. *74*, 219–245.

Gonczy, P. (2008). Mechanisms of asymmetric cell division: flies and worms pave the way. Nat. Rev. Mol. Cell Biol. *9*, 355–366.

Hanada, T., Lin, L., Tibaldi, E.V., Reinherz, E.L., and Chishti, A.H. (2000). GAKIN, a novel kinesin-like protein associates with the human homologue of the *Drosophila* discs large tumor suppressor in T lymphocytes. J. Biol. Chem. *275*, 28774–28784.

Hara, H., Yokosuka, T., Hirakawa, H., Ishihara, C., Yasukawa, S., Yamazaki, M., Koseki, H., Yoshida, H., and Saito, T. (2015). Clustering of CARMA1 through SH3-GUK domain interactions is required for its activation of NF-kappaB signalling. Nat. Commun. *6*, 5555.

Humbert, P.O., Grzeschik, N.A., Brumby, A.M., Galea, R., Elsum, I., and Richardson, H.E. (2008). Control of tumourigenesis by the Scribble/Dlg/Lgl polarity module. Oncogene *27*, 6888–6907.

Johnston, C.A., Hirono, K., Prehoda, K.E., and Doe, C.Q. (2009). Identification of an Aurora-a/PinsLINKER/Dlg spindle orientation pathway using induced cell polarity in S2 cells. Cell *138*, 1150–1163.

Johnston, C.A., Doe, C.Q., and Prehoda, K.E. (2012). Structure of an enzyme-derived phosphoprotein recognition domain. PLoS One *7*, e36014.

Kanai, Y., Wang, D., and Hirokawa, N. (2014). KIF13B enhances the endocytosis of LRP1 by recruiting LRP1 to caveolae. J. Cell Biol. *204*, 395–408.

Knoblich, J.A. (2008). Mechanisms of asymmetric stem cell division. Cell *132*, 583–597.

Knoblich, J.A. (2010). Asymmetric cell division: recent developments and their implications for tumour biology. Nat. Rev. Mol. Cell Biol. *11*, 849–860.

Kulukian, A., and Fuchs, E. (2013). Spindle orientation and epidermal morphogenesis. Philos. Trans. R. Soc. Lond. B Biol. Sci. *368*, 20130016.

Li, Y., Wei, Z., Yan, Y., Wan, Q., Du, Q., and Zhang, M. (2014). Structure of Crumbs tail in complex with the PALS1 PDZ-SH3-GK tandem reveals a highly specific assembly mechanism for the apical Crumbs complex. Proc. Natl. Acad. Sci. USA *111*, 17444–17449.

Li, J., Cai, T., Jiang, Y., Chen, H., He, X., Chen, C., Li, X., Shao, Q., Ran, X., Li, Z., et al. (2015). Genes with de novo mutations are shared by four neuropsychiatric disorders discovered from NPdenovo database. Mol. Psychiatry *21*, 290–297.

Lu, M.S., and Johnston, C.A. (2013). Molecular pathways regulating mitotic spindle orientation in animal cells. Development *140*, 1843–1856.

Lu, M.S., and Prehoda, K.E. (2013). A NudE/14-3-3 pathway coordinates dynein and the kinesin Khc73 to position the mitotic spindle. Dev. Cell *26*, 369–380.

McCoy, A.J., Grosse-Kunstleve, R.W., Adams, P.D., Winn, M.D., Storoni, L.C., and Read, R.J. (2007). Phaser crystallographic software. J. Appl. Crystallogr. *40*, 658–674.

McGee, A.W., Dakoji, S.R., Olsen, O., Bredt, D.S., Lim, W.A., and Prehoda, K.E. (2001). Structure of the SH3-guanylate kinase module from PSD-95 suggests a mechanism for regulated assembly of MAGUK scaffolding proteins. Mol. Cell *8*, 1291–1301.

Morin, X., and Bellaiche, Y. (2011). Mitotic spindle orientation in asymmetric and symmetric cell divisions during animal development. Dev. Cell *21*, 102–119.

Morrison, S.J., and Kimble, J. (2006). Asymmetric and symmetric stem-cell divisions in development and cancer. Nature *441*, 1068–1074.

Otwinowski, Z., and Minor, W. (1997). Processing of X-ray diffraction data collected in oscillation mode. Method Enzymol. *276*, 307–326.

Rodriguez-Boulan, E., and Macara, I.G. (2014). Organization and execution of the epithelial polarity programme. Nat. Rev. Mol. Cell Biol. *15*, 225–242.

Siegrist, S.E., and Doe, C.Q. (2005). Microtubule-induced Pins/Galphai cortical polarity in *Drosophila* neuroblasts. Cell *123*, 1323–1335.

Siller, K.H., and Doe, C.Q. (2009). Spindle orientation during asymmetric cell division. Nat. Cell Biol. *11*, 365–374.

St Johnston, D., and Ahringer, J. (2010). Cell polarity in eggs and epithelia: parallels and diversity. Cell *141*, 757–774.

Tavares, G.A., Panepucci, E.H., and Brunger, A.T. (2001). Structural characterization of the intramolecular interaction between the SH3 and guanylate kinase domains of PSD-95. Mol. Cell *8*, 1313–1325.

Valdar, W.S. (2002). Scoring residue conservation. Proteins *48*, 227–241.

Williams, S.E., and Fuchs, E. (2013). Oriented divisions, fate decisions. Curr. Opin. Cell Biol. *25*, 749–758.

Williams, S.E., Ratliff, L.A., Postiglione, M.P., Knoblich, J.A., and Fuchs, E. (2014). Par3-mInsc and Galphai3 cooperate to promote oriented epidermal cell divisions through LGN. Nat. Cell Biol. *16*, 758–769.

Winn, M.D., Ballard, C.C., Cowtan, K.D., Dodson, E.J., Emsley, P., Evans, P.R., Keegan, R.M., Krissinel, E.B., Leslie, A.G., McCoy, A., et al. (2011). Overview of the CCP4 suite and current developments. Acta Crystallogr. D Biol. Crystallogr. *67*, 235–242.

Yoshimura, Y., Terabayashi, T., and Miki, H. (2010). Par1b/MARK2 phosphorylates kinesin-like motor protein GAKIN/KIF13B to regulate axon formation. Mol. Cell Biol. *30*, 2206–2219.

Zhu, J., Shang, Y., Xia, C., Wang, W., Wen, W., and Zhang, M. (2011). Guanylate kinase domains of the MAGUK family scaffold proteins as specific phospho-protein-binding modules. EMBO J. *30*, 4986–4997.

Zhu, J., Shang, Y., Chen, J., and Zhang, M. (2012). Structure and function of the guanylate kinase-like domain of the MAGUK family scaffold proteins. Front Biol. *7*, 379–396.

Zhu, J., Shang, Y., Wan, Q., Xia, Y., Chen, J., Du, Q., and Zhang, M. (2014). Phosphorylation-dependent interaction between tumor suppressors Dlg and Lgl. Cell Res. *24*, 451–463.

Zhu, J., Shang, Y., and Zhang, M. (2016). Mechanistic basis of MAGUK-organized complexes in synaptic development and signalling. Nat. Rev. Neurosci. *17*, 209–223.